Photon field and energy flow lines behind a circular disc

2014 Phys. Scr. 2014 014039

(http://iopscience.iop.org/1402-4896/2014/T162/014039)

IOP Publishing | Royal Swedish Academy of Sciences Physica Scripta

Phys. Scr. **T162** (2014) 014039 (6pp) doi:10.1088/0031-8949/2014/T162/014039

Photon field and energy flow lines behind a circular disc

D Arsenović[1], D Dimic[2] and M Božić[1]

[1] Institute of Physics, University of Belgrade, Belgrade, Serbia
[2] Faculty of Natural Sciences and Mathematics, University of Niš, Niš, Serbia

E-mail: bozic@ipb.ac.rs

Received 20 September 2013
Accepted for publication 13 March 2014
Published 19 September 2014

Abstract

In order to evaluate electromagnetic energy flow (EME) lines behind a circular disc illuminated by monochromatic laser light, the Rayleigh–Sommerfeld integral is transformed to a simpler form. EME flow lines, interpreted as photon trajectories, explain the change of the intensity pattern with the distance from a circular disc very well, including the Poisson–Arago spot in the center. Possible applications of these results on the study of Poisson–Arago spot experiments with matter beams, are indicated and explained.

Keywords: Poisson–Arago spot, electromagnetic energy flow lines, Rayleigh–Sommerfeld integral, Poisson's spot with molecules

1. Introduction

In recent years there has been a renewed interest in the study, both theoretically and experimentally, of the diffraction of light [1–4] on a circular disc. The famous Poisson–Arago spot [5] from the 19th century discussion about the nature of light, has again attracted the attention of researchers. But during this renewed interest and investigation, researchers are using laser beams, the concepts of the photon [6] and photon wave function [7, 8], and electromagnetic flow lines as possible average photon trajectories [2, 3, 9, 10]. By numerically evaluating electromagnetic energy flow lines behind a circular opaque disc (of radius $R = 5 \cdot 10^{-6}\, m$), illuminated with a monochromatic light (with wavelength $\lambda = R/10 = 500\, nm$), M Gondran and A Gondran [2] found that these lines can reach the bright Poisson–Arago spot that appears at the center of the shadow region generated by such a disc. These authors then argued that for a monochromatic wave in a vacuum, the electromagnetic energy (EME) flow lines correspond to the diffracted rays of Newton's *Opticks*, thus concluding that, after all, Fresnel's wave theory may not be in contradiction with the corpuscular interpretation.

Davidović *et al* [3] evaluated EME flow lines with a larger disk radius ($R = 5 \cdot 10^{-4}\, m$, $\lambda/R = 10^{-3}$) than that used in the work of Gondrans, because larger radii are of practical interest. Namely, Newton used a coin of $R = 10^{-2}\, m$, Arago used metallic disc of $R = 10^{-3}\, m$. In physics textbooks, photos of the diffraction pattern behind a ball of about $R = 1.5 \cdot 10^{-3}\, m$ [11] have been shown. Davidović *et al* [3] also determined the histogram of end points along the axis parallel to the disc at the distance $z = 15\,\text{mm} = 30\,\text{R}$. This histogram agrees very well with the corresponding graph of light intensity as a function of x for given z. This agreement is a new argument supporting the conclusions of M. Gondran and A. Gondran.

Plotting EME flow lines requires a lot of computer time, especially if one wants to use them in explaining experiments in which $\lambda/R < 10^{-1}$. Such experiments are of practical interest, both in photon optics (as above) as well as in matter wave optics. In the Poisson spot experiments with matter waves, which have been possible in recent years [12–17], the ratio of $\lambda/R \ll 10^{-1}$. In the experiments with deuterium molecules, [16] $\lambda/R = 10^{-6}$. In the planned experiment [17] with C_{70}, $\lambda/R = 0.44 \cdot 10^{-6}$. The computer time also increases if one wants to determine EME flow lines up to distance z where the width of the Poisson spot increases so much that the distribution of light intensity becomes flat.

For this reason, in section 2 we simplify the expression for the EM field behind a disc by reducing the well known Rayleigh–Sommerfeld two-fold integral to a one-fold integral. Section 3 is devoted to EME flow lines. Graphs of relative light intensity as functions of transverse coordinates for six distances from the disc of radius $R = 0.5$ mm are given, using the expression for the EM field derived in section 2.

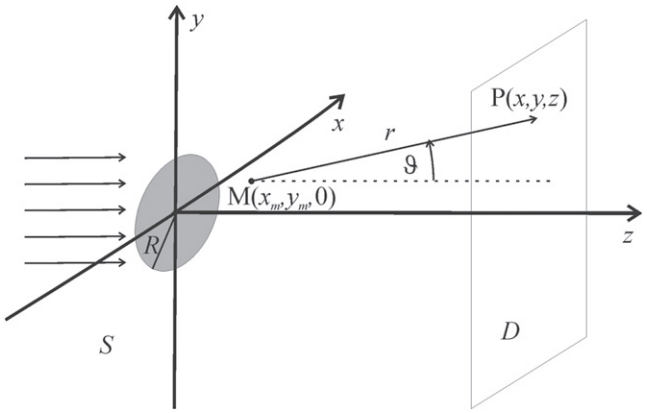

Figure 1. The schematic of the experiment in which monochromatic laser light is scattered on the circular disc.

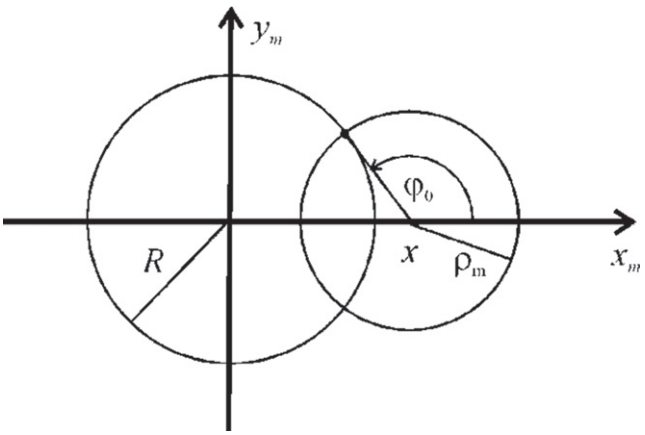

Figure 2. Illustration associated with the derivation of equation (9).

The Poisson spot exists in the Fresnel zone. With increasing distance from the disc, the width of the Poisson spot increases so much that in the Fraunhofer region the graphs of light intensity are flat curves. An analysis of the form of trajectories leads to a clear explanation of this change of the intensity curves with the distance from the disc. In section 4, the possible applications of the results from sections 2 and 3, on the study of Poisson–Arago spot experiments with matter beams [12, 16, 17], are indicated and discussed.

2. Photon fields behind the disc

Let us consider the diffraction of the laser light, described by the monochromatic EM field

$$\left\{\vec{\tilde{E}}(\vec{r},t)=\mathrm{Re}[\vec{E}(\vec{r})e^{-i\omega t}],\quad \vec{\tilde{B}}(\vec{r},t)=\mathrm{Re}[\vec{B}(\vec{r},t)e^{-i\omega t}]\right\},$$

with an incident perpendicular to the opaque circular disc with radius R, lying in the xy plane, with its center located at $(x=0,\ y=0,\ z=0)$ (figure 1). The field behind the disc satisfies Maxwell's free field equations, with the boundary conditions described below. Taking into account the study and arguments of Bialincki-Birula [7], and Raymer and Smith [8] we may consider this Maxwell field as the wave function of a photon from the laser beam diffracted at the disc.

From Maxwell's equations it follows that each component of the space dependent parts of the EM field vectors satisfies [6] the Helmholtz equation

$$\nabla^2 A(\vec{r})+k^2A(\vec{r})=0, \tag{1}$$

where by $A(\vec{r})$ we denoted an arbitrary component of these two vectors $\vec{E}(\vec{r})$ and $\vec{B}(\vec{r})$ and $k=2\pi/\lambda=\omega/c$. For $z<0$ we have $A=A_0e^{ikz}$, and for $z>0$ the solution is given by [1, 2, 5].

$$A(x,y,z)=-\frac{i}{\lambda}\int_S A_0(x_m,y_m)\frac{e^{ikr}}{r}\left(1-\frac{1}{ikr}\right)\cos\vartheta\,dx_m\,dy_m, \tag{2}$$

$$r=\sqrt{(x-x_m)^2+(y-y_m)^2+z^2},\quad \cos\vartheta=\frac{z}{r},\quad k=\frac{2\pi}{\lambda}, \tag{3}$$

where $S=\left\{(x_m,y_m)\middle|x_m^2+y_m^2>R^2\right\}$. Integration is over the $z=0$ plane outside the disk where $A_0(x_m,y_m)$ is determined by the input field, i.e. $A_0(x_m,y_m)=A_0e^{ikz}\big|_{z=0}=A_0$. In addition, $A_0(x_m,y_m)=0$ for $x_m^2+y_m^2<R^2$, because the disc is opaque.

We may now apply the Babinet principle [5]. The field is equal to the difference between a field of a free plane wave, and the one created by illuminating a hole in the $z=0$ plane. Let us denote the latter by $A_h(x,y,z)$, so

$$A(x,y,z)=A_0e^{ikz}-A_h(x,y,z). \tag{4}$$

Therefore, it is sufficient to calculate the integral

$$A_h(x,y,z)=-\frac{iA_0}{\lambda}\int_{S_h}\frac{e^{ikr}}{r}\left(1-\frac{1}{ikr}\right)\cos\vartheta\,dx_m\,dy_m, \tag{5}$$

with $S_h=\left\{(x_m,y_m)\middle|x_m^2+y_m^2<R^2\right\}$. Since the problem possesses cylindrical symmetry, we may choose the point of observation P to be in the xz plane, i.e. to have $y=0$. The two-fold integral in (5) may be reduced to a one-fold integral, as we are going to show. For this reason let us introduce cylindrical coordinates (figure 2) of point M (x_m, y_m, 0) in the plane xy:

$$\rho_m\cos\varphi_m=x_m-x$$
$$\rho_m\sin\varphi_m=y_m. \tag{6}$$

In terms of cylindrical coordinates, the variables r, ϑ and field $A_h(x,0,z)$ read:

$$r=\sqrt{\rho_m^2+z^2},\quad \cos\vartheta=\frac{z}{r} \tag{7}$$

$$A_h(x, 0, z) = -\frac{iA_0}{\lambda}\int_{S_h}\frac{e^{ikr}}{r}\left(1-\frac{1}{ikr}\right)\cos\vartheta\rho_m d\rho_m d\varphi_m. \quad (8)$$

Limits of integration are determined by the area S_h. For a given ρ_m, limits for φ_m are determined by the intersection points of the circle $\rho_m = const$, and the boundary of S_h, which is $x_m^2 + y_m^2 = R^2$. It is straightforward to show that the angles of these two intersection points are φ_0 and $-\varphi_0$, where

$$\varphi_0 = \begin{cases} 0, & X > 1 \\ \arccos X, & -1 \leqslant X \leqslant 1 \\ \pi, & X < -1 \end{cases} \quad (9)$$

with

$$X = \frac{R^2 - \rho_m^2 - x^2}{2x\rho_m}. \quad (10)$$

The cases $X > 1$ and $X < 1$ correspond to combinations of the coordinate x and point (ρ_m, φ_m) when the two circles do not intersect.

The integrand in (8) does not depend on φ_m, so we have

$$A_h(x, 0, z) = -\frac{iA_0}{\lambda}\int_0^{x+R}\rho_m d\rho_m\frac{e^{ikr}}{r}\left(1-\frac{1}{ikr}\right) \times \cos\vartheta\cdot 2\left(\pi - \phi_0\right), \quad (11)$$

where r and ϑ depend on ρ_m by virtue of (7).

Since our problem has cylindrical symmetry, it is convenient to write vectors $\vec{E}(\vec{r})$ and $\vec{B}(\vec{r})$ in cylindrical coordinates. We may assume [2] these vectors in the form

$$\vec{E}(\rho, z) = \left\{e_\rho(\rho, z),\ 0\ , e_z(\rho, z)\right\}$$

and

$$\vec{B}(\rho, z) = \left\{0, b_\varphi(\rho, z), 0\right\}.$$

From Maxwell's fourth equation

$$\nabla\times\vec{\tilde{B}}(\vec{r}, t) = \varepsilon_0\mu_0\partial\vec{\tilde{E}}(\vec{r}, t)\big/\partial t,$$

applied to the monochromatic wave, it follows that

$$\vec{E}(\rho, z) = (ic/k)\left[-(\partial/\partial z)b_\varphi, 0, (\partial/\partial\rho)b_\varphi\right].$$

From Maxwell's third equation

$$\nabla\times\vec{\tilde{E}}(\vec{r}, t) = -\partial\vec{\tilde{B}}(\vec{r}, t)\big/\partial t$$

applied to the monochromatic wave, it follows that $b_\varphi(\rho, z)$ satisfies the Helmholtz equation

$$\nabla^2 b_\varphi + k^2 b_\varphi = 0. \quad (12)$$

For the incident wave we take $\vec{B}_{in}(\rho, z) = \left\{0, A_0 e^{ikz}, 0\right\}$, $\vec{E}_{in}(\rho, z) = \left\{cA_0 e^{ikz}, 0, 0\right\}$. This implies that the boundary condition for $b_\varphi(\rho, z)$ is:

$$b_\varphi(\rho, 0) = \begin{cases} A_0 & \text{for } \rho > R \\ 0 & \text{for } \rho \leqslant R \end{cases}. \quad (13)$$

In the space behind the disc, the function $b_\varphi(\rho, z)$ is just the above given solution of the Helmholtz equation, i.e.

$$b_\varphi(\rho, z) = A_0 e^{ikz} - A_h'(\rho, z), \quad (14)$$

where $A_h'(\rho, z) = A_h(x = \rho, 0, z)$ is given in equation (11).

3. Electromagnetic energy flow lines—average photon trajectories

We saw in the previous section that all six components of the EM field vectors behind the disc are expressed in terms of the function $b_\varphi(\rho, z)$ and its derivatives. This is also the case with the time-averaged EME density:

$$U(\vec{r}) = \frac{1}{4}\left(\varepsilon_0\vec{E}(\vec{r})\cdot\vec{E}(\vec{r})^* + \frac{1}{\mu_0}\vec{B}(\vec{r})\cdot\vec{B}(\vec{r})^*\right) = \frac{b_\varphi b_\varphi^*}{2\mu_0}, \quad (15)$$

and the real part of the time-averaged complex Poynting vector:

$$\vec{S}(\vec{r}) = \frac{1}{2\mu_0}\mathrm{Re}\left[\vec{E}(\vec{r})\times\vec{B}(\vec{r})^*\right] = \frac{1}{2\mu_0}\frac{c\lambda}{2\pi}\mathrm{Im}\left(b_\varphi^*\nabla b_\varphi\right). \quad (16)$$

EME density is transported through space as a flow described by $\vec{S}(\vec{r})$. Formally, this can be expressed as

$$\vec{S}(\vec{r}) = U(\vec{r})\ \vec{V}, \quad (17)$$

where $\vec{V}$ is a local effective velocity vector field, namely the *ray velocity*. This velocity indicates the direction of the EME flow at each space point, and that its magnitude is equal to the EME that crosses, in unit time, an area perpendicular to the flow direction. Combining equations (14), (16) and (17) the velocity field takes the form:

$$\vec{V} = \frac{c\lambda}{2\pi}\frac{\mathrm{Re}\left(A^*\nabla A\right)}{AA^*} \quad (18)$$

In figure 3 we give plots of relative light intensity, $i/i_0 = \left|A^2\right|\big/\left|A_0\right|^2$, as a function of the transverse coordinates for six distances from the disc of radius $R = 0.5$ mm.

In order to calculate the velocity field and the EME flow lines determined by this field, we need the derivatives of A over coordinates. From (11) and (4), and taking into account

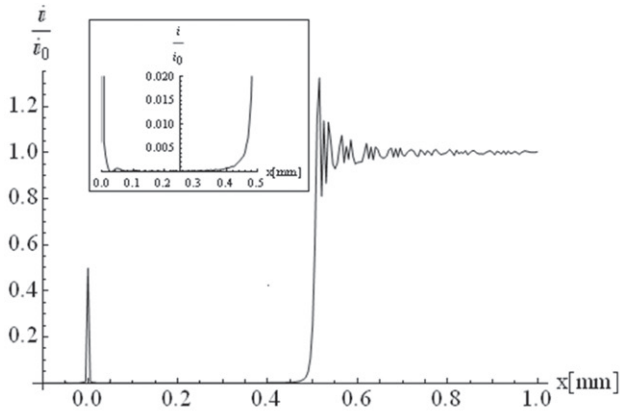

a) $z = 0.0005$ m $= R$

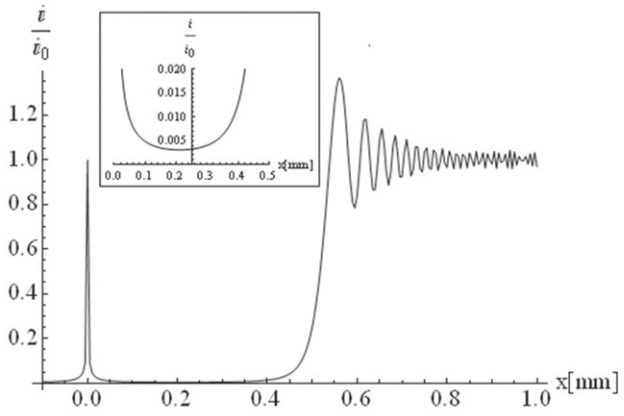

b) $z = 0.01$ m $= 20\ R$

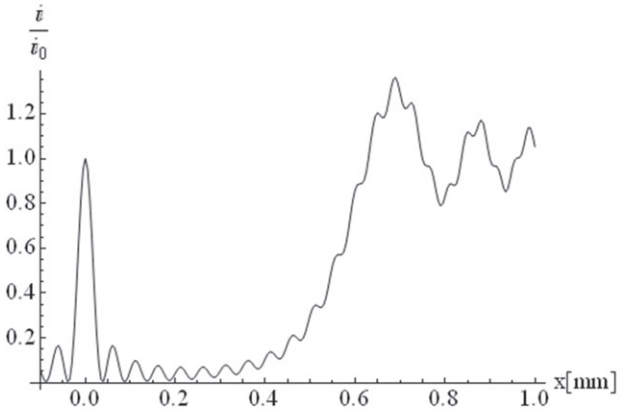

c) $z = 0.1$ m $= 200\ R$

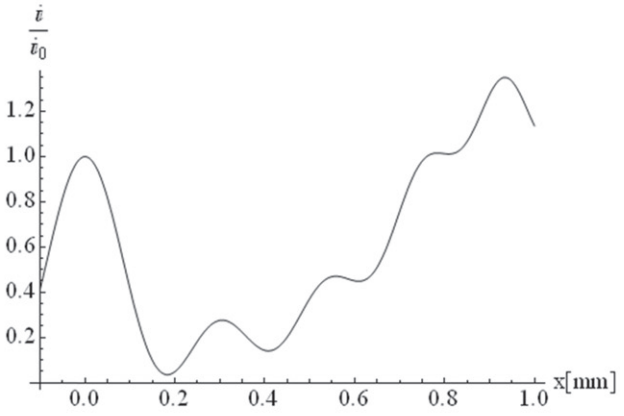

d) $z = 0.5$ m $= 1000\ R$

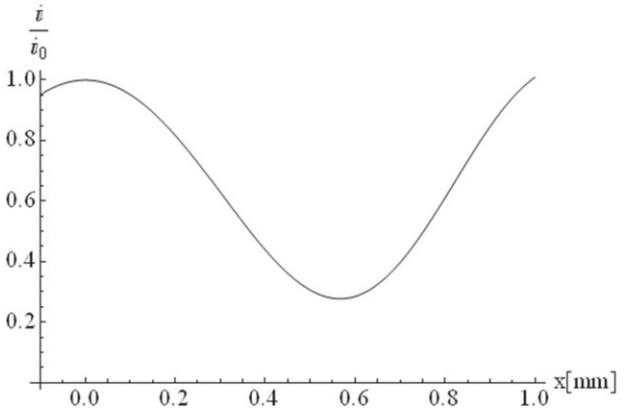

e) $z = 2$ m $= 4000\ R$

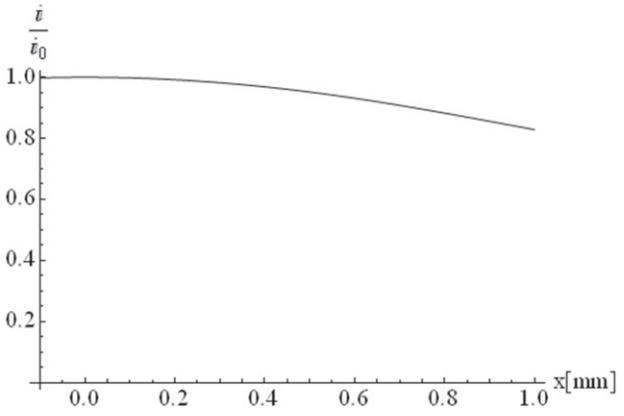

f) $z = 10$ m $= 20\ 000\ R$

Figure 3. Relative intensity of monochromatic light ($\lambda = 500\ nm$) behind a disk of radius $R = 5 \cdot 10^{-4}\ m$ as a function of transversal coordinate x, at six distances z from the disk: (a) $z = 0.0005$ m, (b) $z = 0.01$ m, (c) $z = 0.1$ m, (d) $z = 0.5$ m , (e) $z = 2$ m, (f) $z = 10$ m.

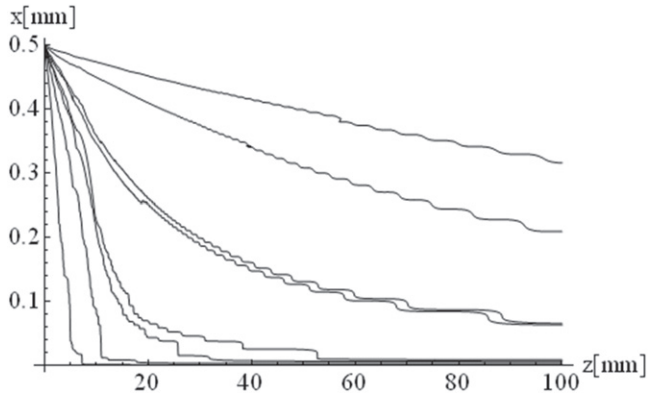

Figure 4. Eight EME flow lines behind the disc of radius $R = 0.5$ mm ($\lambda/R = 10^{-3}$).

that r depends only on z while φ_0 depends only on x, we have

$$\frac{\partial A_h}{\partial x} = -\frac{iA_0}{\lambda}\int_0^{x+R}\rho_m d\rho_m \frac{e^{ikr}}{r}\left(1-\frac{1}{ikr}\right) \times \cos\vartheta \cdot 2\frac{\partial}{\partial x}(\pi-\varphi_0) \tag{19}$$

$$\frac{\partial A_h}{\partial z} = -\frac{iA_0}{\lambda}\int_0^{x+R}\rho_m d\rho_m \frac{\partial}{\partial z}\left[\frac{e^{ikr}}{r}\left(1-\frac{1}{ikr}\right)\cos\vartheta\right] \times 2(\pi-\varphi_0) \tag{20}$$

$$\frac{\partial A}{\partial x} = -\frac{\partial A_h}{\partial x}, \frac{\partial A}{\partial z} = ikA_0 e^{ikz} - \frac{\partial A_h}{\partial z}. \tag{21}$$

Eight EME flow lines are drawn in figure 4 by evaluating A_h, $\frac{\partial A_h}{\partial x}$ and $\frac{\partial A_h}{\partial z}$ numericallyfor the disc radius $R = 0.5$ mm $\left(\lambda/R = 10^{-3}\right)$. The form of these EME flow lines is *grosso modo* similar to the form of EME flow lines given for $R = 5\,\mu m$ in figure 6 in [2] and in figure 4 in [3]. All these sets of EME flow lines, interpreted as photon trajectories, explain the change of the intensity pattern with the distance from a circular disc very well, including the Poisson–Arago spot in the center. The trajectories which start very near the disc edge (figure 4), for example at

$$x_i = 0.00050001\ m + i \cdot 10^{-8}\ m,\ i = 1,2,3,4,5,6,7,8,9,$$

deflect towards the optical axis, at the distance $z \cong R$, giving rise to the central maximum having the value $i/i_0 = 0.5$, in agreement with the following formula for the relative light intensity along the axis, derived by Sommerfeld [5]:

$$\frac{i}{i_0} = \frac{\left(\frac{z}{R}\right)^2}{1+\left(\frac{z}{R}\right)^2}. \tag{22}$$

This central maximum increases with increasing z, until it reaches a value very close to 1 (for $z/r = 5, i/i_0 = 0.96$). The value of the maximum remains at 1 with further increases of z, as seen on in the intensity curves in figures 3(b)–(f), in agreement with relation (22). The deflection of trajectories decreases with increasing distance from the disc of the initial point. One also notes the steps in the trajectories, and the length of steps increases with increasing distance of the initial point. Eventually these trajectories reach the region of the Poisson spot and contribute to the widening of the central maximum with increasing z, in accordance with the graphs of relative intensity, seen in figures 3(c)–(e). At very large distances, $z/R \geqslant 2 \cdot 10^4$, the intensity curve is almost constant (figure 3(f)). We see that the central maximum becomes so wide that it is not pronounced any more at the distance $z_c = R^2/\lambda = 0.5\ m$, determined by $N \equiv (R^2/z_c\lambda) < 1$, where N is the Fresnel number. At the distances $z \gg z_c$ the intensity pattern looks like the unobstructed intensity pattern.

4. Matter waves and trajectories behind a circular disk

In describing the diffraction of a matter particle on a circular disc, one starts with the Schrodinger equation for a particle's wave function $\Psi(\vec{r}, t) = e^{-i\omega t}\psi(\vec{r})$. One is faced again with the problem of solving the Helmholtz equation for $\psi(\vec{r})$ with the same boundary and initial conditions. The only difference is that for a particle with mass m and velocity v, the relations $\hbar k = mv$ and $\omega = \hbar k^2/2m$ are applicable, instead of the relation $c = \omega/k$, which is associated with light/photons. Therefore, the matter field behind the disc is given by equation (4), where A_h is given by equation (11).

The equation of the particle trajectory, the so called Bohmian trajectory, is determined by the quantum mechanical current, that is:

$$\frac{d\vec{r}}{dt} = \frac{i\hbar}{2m}\frac{\Psi\nabla\Psi^* - \Psi^*\nabla\Psi}{\Psi^*\Psi} = \frac{i\hbar}{2m}\frac{A\nabla A^* - A^*\nabla A}{A^*A}. \tag{23}$$

Evidently, the latter equation has the same form (up to a constant factor) as equation (18) for a photon trajectory. In other words, the Poynting vector associated with the photon field plays the same role as the quantum mechanical probability current density of a massive particle [9].

This implies that the simplified form (11) of the Rayleigh–Sommerfeld formula might be useful for the study of analogous experiments with matter beams [12–17]. The Poisson–Arago spot was detected recently in experiments with deuterium molecules [16], and experiments with C_{70} have been planned [17]. The goal of this experiment is to demonstrate the quantum mechanical wave nature of increasingly larger and more massive particles [17]. In the experiment with deuterium molecules, $\lambda/R = 10^{-6}$. In the planned experiment [17] with C_{70} this ratio would be $\lambda/R = 0.44 \cdot 10^{-6}$. For such small values of the ratio λ/R, it is desirable and useful to have a simpler expression for the wave function, which we achieved by deriving expression (8).

The demonstration of quantum-mechanical interference of larger molecules is motivated by, amongst others, the desire to understand the transition from the quantum-mechanical regime to the classic regime. From this perspective, the approach to the Poisson spot experiment, proposed and elaborated here, might be useful because it lies somewhere in between the standard quantum mechanical approach and the classical approach. In this approach, the wave field is determined, from Schrodinger's equation, as the basic equation of standard quantum mechanics. In addition, the trajectories, determined by the quantum mechanical current, are introduced. These trajectories differ from classical trajectories because they are determined by the wave function. So, this approach makes it possible to study the transitions from quantum-mechanical to classical regimes, by studying how quantum mechanical trajectories, Bohmian trajectories, approach classical trajectories with increasing mass. It is also possible to study the influence of van der Waals' force, using Bohmian trajectories, and to compare the results with the calculations from [17], performed using a formula equivalent to the original form of the Rayley-Sommerfeld formula, with an added van der Waals phase term.

Acknowledgment

D Arsenović and M Božić, acknowledge support from the Ministry of Education and Science of Serbia under projects III45016 (AD and MB) and OI171028 (MB).

References

[1] Lucke R L 2006 *Eur. J. Phys.* **27** 193
[2] Gondran M and Gondran A 2010 *Am. J. Phys.* **78** 598
[3] Davidović M, Sanz A S, Božić M, Arsenović D and Dimić D 2013 *Phys. Scr.* **T153** 014015
[4] Emile O, Voisin A, Niemiec R., Viaris de Lesagno B, Pruvost L, Ropars G, Emile J and Brousseau C 2013 *Europ. Phys. Lett.* **101** 54005
[5] Sommerfeld A 1964 *Optics* vol 4 (New York London: Academic)
[6] Saleh B E A and Teich M C 2007 *Fundamentals of Photonics* (Hoboken, NJ: Wiley)
[7] Bialincki-Birula I 1994 *Acta Phys. Pol.* **86** 97
[8] Smith B J and Raymer M G 2007 *New J. Phys.* **9** 414
[9] Davidović M, Sanz A S, Arsenović D, Božić M and Miret-Artes S 2009 *Phys. Scr.* **T135** 014009
[10] Sanz A S, Davidović M, Božić M and Miret-Artés S 2010 *Ann. Phys.* **325** 763
[11] Young H D and Freedman R A 1996 (Rading, MA: Addison-Wesley)
[12] Juffmann T, Nimmrichter S, Arndt M, Gleiter H and Hornberger K 2012 *Found. Phys.* **42** 98
[13] Komrska J 1971 *Advances in Electronics and Electron Physics* (New York: Academic) pp 139–234
[14] Matteucci G 1990 *Am. J. Phys.* **58** 1143
[15] Nowak S, Stuhler N, Pfau T and Mlynek J 1998 *Phys. Rev. Lett.* **81** 5792
[16] Reisinger T, Patel A A, Reingruber H, Fladischer K, Ernst W E, Bracco G, Smith H I and Holst B 2009 *Phys. Rev.* **79** 053823
[17] Reisinger T, Bracco G and Holst B 2011 *New J. Phys.* **13** 065016